remote sensing

MDPI

Article

Mapping Inter-Annual Land Cover Variations Automatically Based on a Novel Sample Transfer Method

Cheng Zhong [1], Cuizhen Wang [2], Hui Li [3,*], Wenlong Chen [1] and Yong Hou [1,*]

1 Three Gorges Research Center for Geo-hazard, Ministry of Education, China University of Geosciences, Wuhan 430074, China; zhonglxm@cug.edu.cn (C.Z.); wlchen_cug@sohu.com (W.C.)
2 Department of Geography, University of South Carolina, 709 Bull St., Columbia, SC 29208, USA; cwang@mailbox.sc.edu
3 School of Earth Science, China University of Geosciences, Wuhan 430074, China
* Correspondence: rslihui@cug.edu.cn (H.L.); yonghou93@sohu.com (Y.H.); Tel.: +86-138-0861-8138 (H.L.); +86-158-2730-1696 (Y.H.)

Received: 8 August 2018; Accepted: 5 September 2018; Published: 12 September 2018

Abstract: Most land cover mapping methods require the collection of ground reference data at the time when the remotely sensed data are acquired. Due to the high cost of repetitive collection of reference data, however, it limits the production of annual land cover maps to a short time span. In order to reduce the mapping cost and to improve the timeliness, an object-based sample transfer (OBST) method was presented in this study. The object-based analysis with strict constrains in area, shape and index values is expected to reduce the accident errors in selecting and transferring samples. The presented method was tested and compared with same-year mapping (SY), cross-year mapping (CY) and multi-index automatic classification (MI). For the study years of 2001–2016, both the overall accuracies (above 90%) and detailed accuracy indicators of the presented method were very close to the SY accuracy and higher than accuracies of CY and MI. With the presented method, the times-series land cover map of Guangzhou, China were derived and analyzed. The results reveal that the city has undergone rapid urban expansion and the pressure on natural resources and environment has increased. These results indicate the proposed method could save considerable cost and time for mapping the spatial-temporal changes of urban development. This suggests great potential for future applications as more satellite observations have become available all over the globe.

Keywords: land cover; remote sensing; automatic classification; sample transfer; object-based analysis

1. Introduction

Currently, more than 50% of the world's population live in cities and this figure is projected to reach 67.2% in 2050 [1]. Along with the rapid growth of population concentrations and economic activities being intensified, the demand for developed land increased dramatically, manifesting as urbanization [2]. Global urban areas have been rapidly expanding, especially in developing countries. The prospect is that the urbanization rate will reach 60% by 2030 [1]. The conversion of rural areas into urban areas through development is currently proceeding more quickly in developing countries than in the developed world, for example, in China, India, Vietnam and Bangladesh [1–6]. Urban expansion inevitably converts the natural and semi-natural ecosystems into impervious surfaces and thus become the most widespread anthropogenic causes of increased environmental degradation, such as natural vegetation cover decline and arable land loss, urban heat islands, air pollution, hydrological circle alteration and biotic homogenization [3–6]. Although urban land covers only less than 3% of the global terrestrial surface, their marked effects on environmental conditions becomes increasingly serious and is generating increasing attention globally [5–7].

Since urban ecosystems are strongly influenced by anthropogenic activities, considerably more attention is currently being directed towards monitoring urban land cover variations, which is not only crucial for characterizing the ecological consequences of urbanization but also for developing effective economic, social and environmental policies in order to mitigate expansion's adverse impacts [5]. A considerable amount of research has been conducted all around the world to understand the spatial patterns [1,3,6], driving forces [8] and the ecological and social consequences of urban expansion [7,9]. Among them, identifying and understanding the driving factors of urban expansion is crucially important for the design of effective urban planning and management strategies [8]; monitoring pattern changes could help characterize the ecological consequences of urbanization, as discussed above. Therefore, considerable literatures have paid attention to monitoring land cover changes [4–7,9,10].

Remote sensing has been widely recognized as a powerful and cost-effective way to study historical land cover dynamics and to relate their patterns to environmental and human factors [11–15]. Although supervised classification methods have been successfully employed for mapping urban land cover dynamics in recent decades [16,17], such mapping efforts still rely on collecting ground reference data for each classification. As images subject to different conditions (e.g., illumination, viewing angle, soil moisture and topography), they are not stationary over time or space. Such differences can affect the observed spectral signatures of the land-cover types, thus the classification algorithms and parameters assigned for the input data at a certain time are probably not suitable for data from another time, no matter how well they are developed [18]. This makes it difficult and expensive for mapping land cover dynamics with times-series imagery.

Many efforts have been made to reduce the mapping cost and improve the timeliness of the map products [19–22]. Decades ago, the idea of classifier extension or generalization was first proposed, which aimed at finding a training set or a trained classification algorithm that can be utilized repeatedly for multiple years without the need for year-to-year reformulation [19]. Temporal inputs, such as the shape of time-series trajectory of vegetation indices extracted from multi-temporal imagery, were involved in related studies [20–22]. However, successful examples are rare and mostly in natural vegetation environments [22–25]. Alternatively, remote sensing index-based methods have been developed, considering that the indices are often effective to highlight certain land cover type from others [26–28]. In recent studies [29,30], an automatic strategy to map typical urban land cover, that is, water, bare land, built-up, forest and cropland, has been presented with modified normalized difference water index (MNDWI) [26], normalized bare land index (NBLI) [29] and the urban index (UI) [31]. With these indices, the thresholds for extract land cover types were assigned to an unsupervised classifier, avoiding the iterative trial-and-error optimization process. In Reference [32], four land cover types were mapped automatically with MNDWI, normalized difference vegetation index (NDVI) [33] and the biophysical composition index (BCI) [34] and the multilevel Otsu's thresholding method [35]. Unfortunately, both the type and number of indices available for automatic land cover mapping have been limited.

From another point of view, the analysis of remote sensing images captured at different dates could be considered as a Transfer-learning (TL) problem [36], particularly, a domain adaption (DA) issue [37,38]. Images acquired in the same area at different time instants are associated with the source domain and target domain, respectively [39]. Here, the source domain indicates the image associated with prior knowledge or classified samples, target domain represents images needed to be classified. In this study, it is believed the associated joint probability distributions of the two domains are different but close enough, thus the source-domain information can help solve the target-domain learning problem. However, errors (accident errors or human errors, etc.) in the process of sample selection in source domain will probably affect the classification accuracy in the target domain, when mapping with transferred samples.

This study aims to improve the accuracy of mapping land cover variations without current samples, based on an object-based sample transfer (OBST) method with strict constrains in area, shape and index value. There, object-based sampling and change detection algorithms were developed in the process of sample selection and sample transfer, respectively. Its results were carefully compared with those from SY, CY and MI. At last, characteristics and potential applications about the proposed strategy were discussed.

2. Materials

2.1. Study Site

Guangzhou is the third most populated city in mainland China, following Beijing and Shanghai. As shown in Figure 1, the city is located in the downstream reaches of the Pearl River, about 120 km north-northwest of Hong Kong and 145 km north of Macau. The city covers 7434.4 square kilometers along the river from 112°57′ to 114°03′E and 22°26′ to 23°56′N in south-central Guangdong province [40]. In 2016, the city was estimated to have a population of 14.04 million, making it one of the most populous megacities on Earth. The migrant population from other parts of China comprised about 40% of the city's total population. The GDP reached ¥1961.1 billion (US $295.4 billion) and GDP per capita was ¥145,254.4 (US $21,868.1) [40]. For the three consecutive years of 2013–2015, Forbes ranked Guangzhou as the best city for business in the Chinese mainland. However, due to the rapid industrialization, it is also considered one of the most polluted cities. Despite being located just south of the Tropic of Cancer, Guangzhou has a humid subtropical climate that is influenced by the East Asian monsoon. The primary land cover types in the city are built-up, forest, water, bare land and cropland.

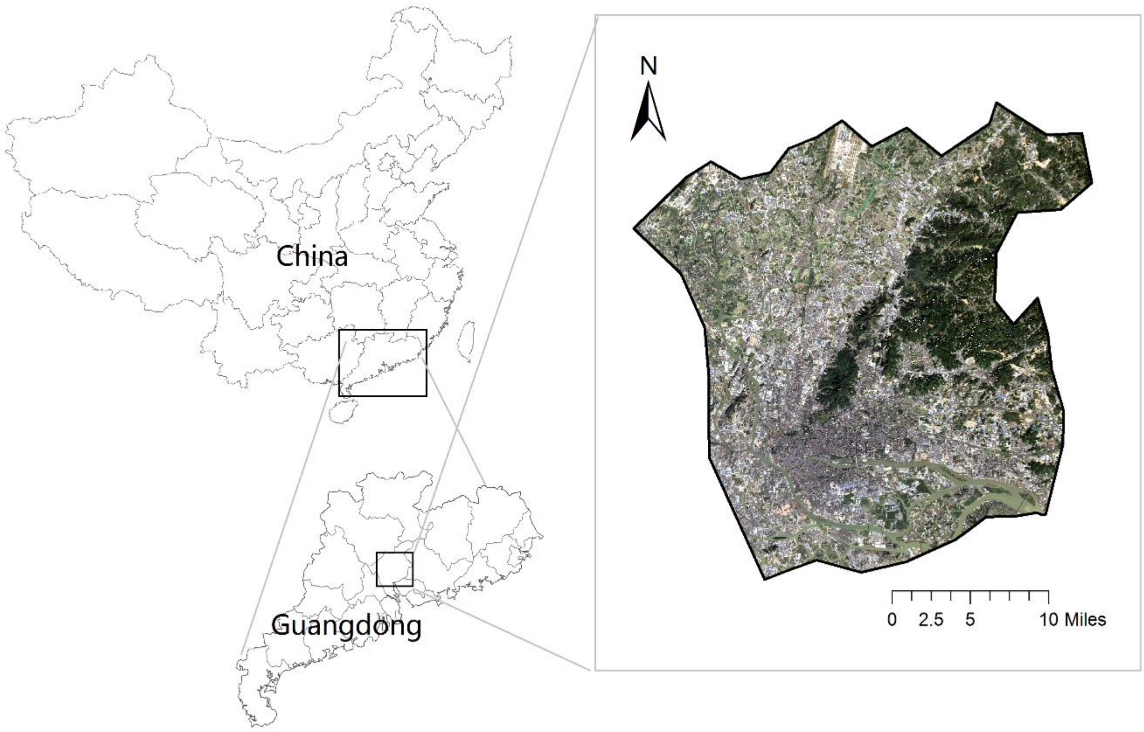

Figure 1. The city of Guangzhou in Guangdong province, China, is the area of interest of this study.

As one of the fastest developing cities in China, Guangzhou underwent dramatic expansion in the past decades. In previous studies, the land cover change in Guangzhou from 1998 to 2003 was comprehensively analyzed based on Landsat Thematic Mapper (TM)/Enhanced Thematic Mapper Plus (ETM+) imagery [41]. The relationship between land surface temperature and land cover in the city and the rainfall-runoff relationship in the rapid growing metropolitan area was estimated with remotely sensed variables [42]. A study monitoring annual urbanization activities in Guangzhou using Landsat images from 1987 to 2015 was reported [32], where a multiple-indices strategy was employed for automatic land cover classification.

2.2. Data

Landsat images covering the city (Path: 122, Row: 44) were carefully selected (Table 1). The data were downloaded from the NASA Landsat data collection, with special consideration of cloud cover, phenology and dryness of ground. In this study, the Landsat Thermal Infrared Sensor (TIRS) bands were rescaled to 30 m prior to building an index image.

Table 1. Landsat images used in this study.

Capture date	Sensor	Bands	Spatial Resolution (m)	Cloud Amount (%)
30 December 2001	TM	7	30	0.01
4 December 2003	TM	7	30	3.00
28 December 2006	TM	7	30	0.01
2 November 2009	TM	7	30	0.00
2 November 2011	ETM+	8	30	0.04
15 October 2014	OLI&TIRS	11	30	7.65
7 February 2016	OLI&TIRS	11	30	2.44

An independent set of IKONOS images covering the study site in corresponding year was collected from Guangzhou Land Resource and Planning Commission and served as the validation source. It is believed the manually interpreted results from the images could represent the ground truth very well, due to its very high spatial resolution (1 m). Besides, administrative maps, climate and environmental data were collected from the Guangzhou Municipal Environmental Protection Bureau. Related social, commercial and transportation data came from the Guangzhou Statistical Yearbook.

With the failure of scan line corrector (SLC) of the Landsat Enhanced Thematic Mapper Plus (ETM+) sensor since 2003, about 22% of an SLC-off image scene is not scanned. To improve the usability of the ETM+ SLC-off data, multi-temporal Landsat images (other images in 2011, 2012 and 2013) were used as referable information by building a regression model between the corresponding pixels [43]. Atmospheric correction of the Landsat images listed in Table 1 was implemented by the Fast Line-of-sight Atmospheric Analysis of Hypercubes (FLAASH) model in ENVI 5.3 [30]. Digital numbers at each pixel were converted to surface reflectance through this process.

3. Methods

Our primary interest was to map the urban land cover variations. Among the five land cover classes in this study, The built-up is defined as built environment with impervious surfaces dominated by man-made structures such as buildings and transportation facilities; water includes areas of open water such as rivers and ponds; bare land includes exposed soil surfaces with little vegetation cover such as deforested land, abandoned farmland, quarries and naturally non-vegetated areas; forest represents the woodlands; and cropland mainly includes herbaceous areas that are covered with shrubs, grass, farmland and orchard.

As the training set is only available in the source domain (images classified), this study focuses on how to transfer the labeled samples to the target domain (images unclassified) reliably. In order to reduce the accident errors in the process of sample selecting and transferring, the OBST method is presented. The main idea and flowchart of the method are shown in Figure 2 and described in following subsections.

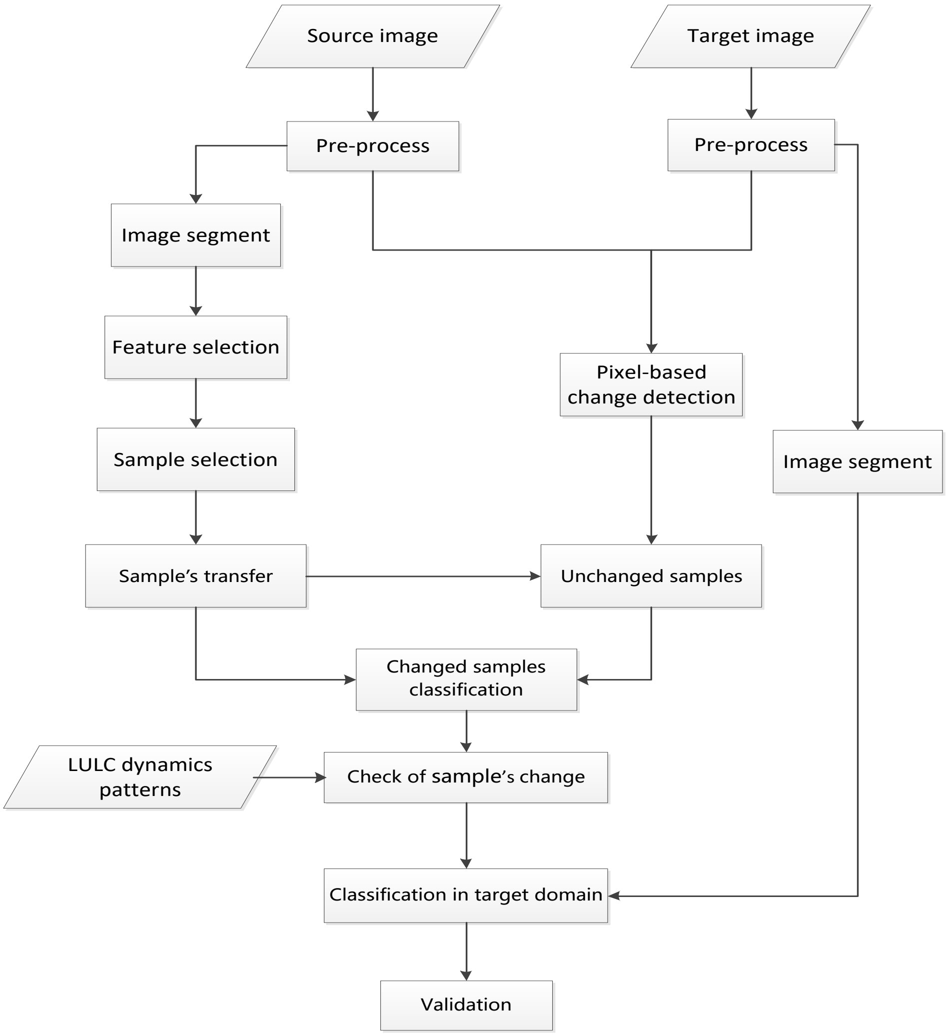

Figure 2. The flowchart of the presented method.

Firstly, a multi-resolution segmentation (MRS) is carried out, as the first step and a necessary prerequisite for the automatic object-based analysis.

Secondly, tens of spectral, geometric and texture features are developed to depict land cover objects comprehensively, followed by a feature selection step to reduce insignificant features.

Thirdly, an object-based sampling method is presented, with strict constrains in area, shape and index value, to reduce sample selection errors.

Then, an object-based change detection (CD) is put forward, where sample's change could be detected according to the proportion of changed or unchanged pixels within the sample, constrained by the general patterns of land cover variations.

At last, a supervised classification with transferred samples in target image is carried out and then compared with SY mapping, CY mapping and MI classification.

3.1. Image Segmentation

The multi-resolution segmentation (MRS) is probably the most popular and important segmentation algorithm, among all related methods [44,45]. The vital step of image segmentation is to select the input layers and specify their weights. In this study, the Landsat multispectral images were set as the input, as the spectral profile recorded by the images is an important feature for depicting a land cover type [46,47]. The weights of shape/color and compactness/smoothness were first determined based on experience [48–50]. The weights of shape were selected from 0.1 to 0.5 with a step of 0.05 and those of color from 0.9 to 0.5. The weights of compactness and smoothness were both fixed as 0.5.

Here, five land cover types were analyzed: built-up, forest, water, bare land and cropland. Some land surfaces such as paddy fields and fallow cropland are either indistinct or difficult to distinguish from water and bare lands, respectively. Therefore, the trial-and-error method was used to select the suitable scale parameter to depict the image segments [51–53]. It was found that the weights of 0.1 for shape and 0.9 for color were more suitable.

3.2. Feature Definition and Selection

In order to depict image objects comprehensively, tens of spectral, geometric and texture features were initially selected based on experts' knowledge and experience, as shown in Table 2. The spectral information is vital for depicting image objects. In this study, two spectral features, the mean and standard deviation of grey values of all pixels of an image object, were selected. It has been demonstrated that geometric features are of great help for identifying man-made objects or linear objects [54]. Here, the length-width ratio, shape index and the number of corner points of image object were involved and calculated. Texture analysis based on local spatial variation of intensity or color brightness serves an important role in OBIA and the extracted texture features directly affect the quality of subsequent processing [55]. The gray level co-occurrence matrix (GLCM) has been extensively applied in texture description [56], showing that its results are better than other texture discrimination methods [57,58]. In this study, several GLCM based texture features were involved (Table 2).

Table 2. The features of objects.

No.	Name	Description	No.	Name	Description
01–07	B1_mean ... B7_mean	Band 1 mean ... Band7 mean	21	NCorPts	The number of corner points
08–14	B1_dev ... B7_dev	Band 1 Std ... Band7 Std	22	GLCM_1	Homogeneity
15	Len	The length of objects	23	GLCM_2	Contrast
16	wid	The width of objects	24	GLCM_3	Variance
17	L-W ratio	The length-width ratio	25	GLCM_4	Angular second moment
18	Compact	The compactness	26	GLCM_5	entropy
19	BorderLen	The border length	27	GLCM_6	Correlation
20	ShapeIn	The shape index			

Feature selection is often required to reduce redundant data when analyzing high-dimensional datasets. A wrapper feature selection method based on the RF algorithm [59,60] was applied to pick up useful features from the feature pool.

3.3. Sample Selection

Within a type, the geometric shapes and sizes of image objects vary dramatically. According to Tobler's first law of geography [61], the center of small or narrow object is more likely affected by surrounding objects, namely it is probably a mixed pixel. In contrast, the center part of bigger and wider objects might be immune to surrounding influences and represents real land cover. Thus, bigger and wider objects become preferred candidates. For this, a series of geometric criterions, including the length-width ratio <8, area > the average and the number of corner points < 50, were involved to seek interested candidates.

According to previous study [30,32], pixels with higher index values could represent corresponding land cover well. Thus, index value was imported as another criterion. To reduce noises or errors, an index value range from $[+\sigma]$ to $[+3\sigma]$ was designed, in which E and σ were the average and standard deviation of the index image, respectively.

Objects satisfied above criterions were first selected as candidates and then samples were randomly picked up from the candidate pool. With strict constraints in area, shape and index value, it is expected to reduce accident errors and human errors in sample selection. Besides, it is believed that those samples could also reflect land cover variation better.

3.4. Sample' Transfer

There are two cases for inter-annual samples' transfer: (1) keep unchanged, (2) change to other type. In order to detect the sample's change, change detection (CD) technique was imported. As labeled samples are not available in target domain, it is hard to apply post-classification CD here. Considering a sample may change partly, pixel-based CD should be implemented first, then sample's status could be determined according to the proportion of changed pixels within the object. among them, note that it is always necessary, but often difficult, to assign a suitable threshold value to differentiate change from no change precisely and research often suffers from the mis- or over-detection of changes [62,63], as a lower threshold may exclude areas of change and a high value includes too many areas of change.

According to above discussion, a principle component analysis (PCA) was applied at first to detect pixel's change, in association with an unsupervised classifier (K-means) for assigning the threshold (for judging change or no change) automatically [32]. Then, a sample's status was determined if more than 80% of its pixels were changed or unchanged. Otherwise, its status was thought to be unclear and would not be involved in later process.

In the CD results, the locations of changed and unchanged samples were recorded. Here, unchanged samples transfer the labeled information from the previous image to the new image, while the changed samples reflect the land cover changes. For the changed samples, their types in the target image were reassigned with a random forest classifier trained with unchanged samples. After that, samples' change was further checked with the general patterns of land cover variations.

3.5. Classification and Performance Evaluation

In this study, a non-parametric ensemble learning method for classification, the random forest is employed for all supervised classifications, as it has been widely used in related fields with excellent performance [64,65]. Here, 60% of transferred sample was considered as the training sets and the remaining 40% of samples as the test sets. Both the training sets and the selected feature subsets were used to train the RF models and then classify the test sets. The mean and stdev values of the accuracies were obtained from 50 random runs.

In order to evaluate the performance of the presented method, several related methods were also involved as comparison, including: (1) supervised classification with training and validation samples from the same year, namely single-year mapping (SY); (2) supervised classification with training samples and test sets from different years, namely cross-year mapping (CY); and (3) multiple-indices based classification (MI) [30]. As shown in Table 1, Landsat images of Guangzhou in 2001, 2003, 2006, 2009, 2012, 2014 and 2016 were used in the experiments. Confusion matrices and kappa coefficients were employed to evaluate the accuracies, with the reference data manually interpreted from IKONOS images covering the study site in corresponding years. Furthermore, the drivers of land cover variation and the interaction between it and surroundings during the study year will be discussed, with related climate, environmental, social, commercial and transportation data.

4. Results

4.1. The Process of Presented Method

The process of the presented method, including image segmentation, sampling, change detection, sample transfer and object-based classification, is illustrated in Figure 3. Only a subset of the study site (Figure 3a) is displayed for better visualization.

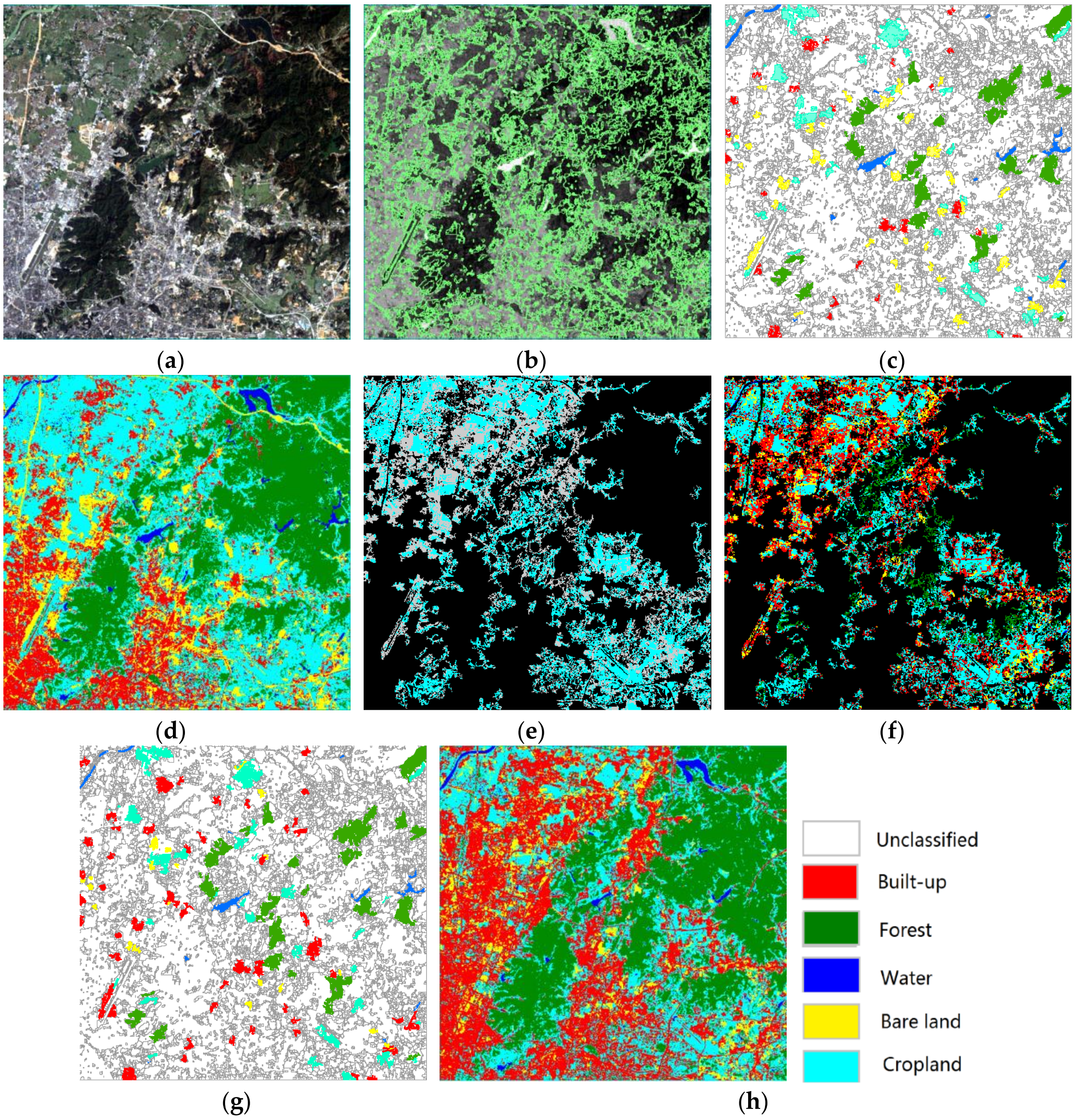

Figure 3. The process of the presented method. (**a**) partial Landsat image in 2001, (**b**) image objects in vector overlaid on the MNDWI image, where brighter tone indicates higher index value; (**c**) labeled samples overlaid on the segment image; (**d**) classification result in 2001, (**e**) detecting the change of cropland between 2001 and 2016, (**f**) relabeling the changed cropland, (**g**) transferred samples for the 2016 image and (**h**) classification result in 2016.

In Figure 3b, the MNDWI image was used as background, to show if the segmentation results match index images well. Then, samples were selected with constrains in geometric shape and index value introduced in Section 3.3 and shown in Figure 3c. To demonstrate the process of change detection, a single type of cropland and its samples with clear changes are involved in Figure 3e,f. Namely, objects within which the proportions of change or unchanged pixels are less than 80% are not shown in figures. In Figure 3e, the grey polygons suggest that cropland is changed to other types. Note it makes up a significant part of the original distribution. After the relabeling step, the new land cover types become clear (Figure 3f). Clearly the changed croplands were mostly converted to built-up, with some changing to bare land and forest. This reflects the primary tendency of urban land cover dynamics to some extent. Based on the change detection result, sample's change was detected Figure 3g Compared with Figure 3c, many bare land samples have changed to built-up, several crop samples have changed to built-up and bare land, while water and forest sampled remained relatively stable. Consequently, the number of built-up sample has increased remarkably, bare land samples and cropland samples have decreased respectively and others keep unchanged. The classification result with the transferred samples is shown in Figure 3h, which also reveals dramatic increase of built-up areas from 2001 to 2016.

4.2. Validation and Comparison

In order to evaluate the performance of the proposed method, experiments on Landsat images of Guangzhou in 2001, 2003, 2006, 2009, 2012, 2014 and 2016 were implemented. Furthermore, the SY, CY and MI classifications were carried out for comparison analysis. Related results are shown in Figure 4, Tables 3 and 4.

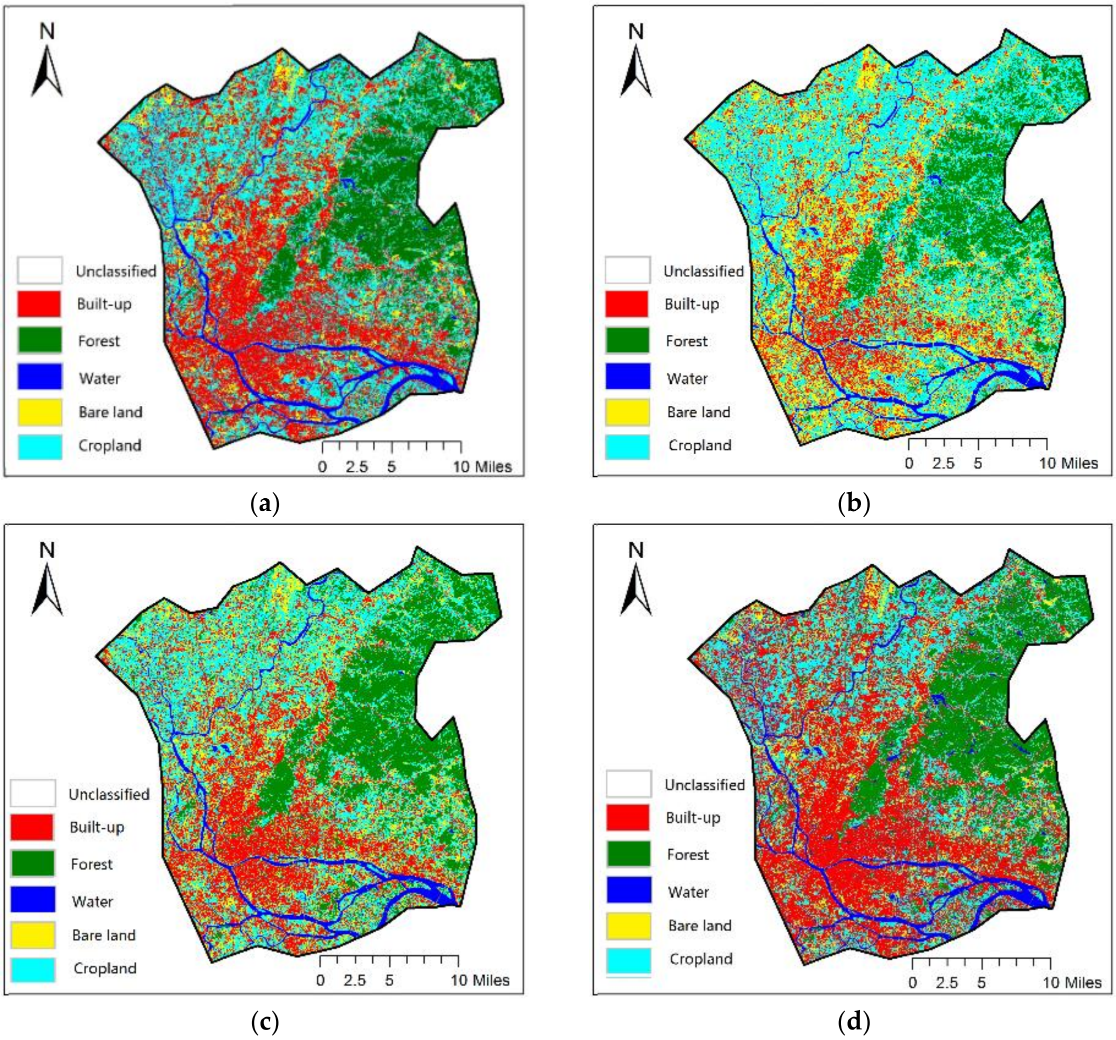

(**a**) (**b**) (**c**) (**d**)

Figure 4. The land cover maps in 2016. (**a**) SY result, (**b**) CY result with samples from the 2001 image, (**c**) MI result and (**d**) OBST result.

Using the classification of the 2016 image as example (Figure 4), the MI and OBST results are visually close to the SY result, while the CY result is much different. Specifically, the built-up area in the CY result (470 km^2) is much less than the SY result (560 km^2) and the difference is mainly due to the misclassification of built-up into bare land. This tells that mapping with samples from a previous year cannot efficiently reflect the dramatic urban expansion in a rapidly developing city.

Table 3. Overall accuracies for 2001–2016.

Method \ Year	2001	2003	2006	2009	2012	2014	2016
SY	94.39	94.55	93.33	94.99	94.12	93.08	95.37
MCY *	81.57	84.60	83.35	86.95	86.70	81.28	84.63
MI	88.95	89.66	86.15	87.97	85.82	88.45	87.35
OBST	91.62	90.74	92.81	91.43	91.54	92.03	93.56

* MCY indicates the mean cross year mapping at the year.

In Table 3, all SY accuracies are higher than 93%, suggesting that supervised classification is able to achieve a very high accuracy with training data collected in the same year as image acquisition. When performing classification with samples from different years, the MCY accuracy (about 82–87% in different years) is about 10% lower than SY. Note that the higher MCY values are located at the middle of this row, as the mean time difference between 2009 and the other years is the least. The MI accuracies (about 88%) are higher than the MCY accuracies and close to the SY accuracies. The OBST accuracies are higher than 90%, only slightly lower than the SY accuracy. The above results suggest that the presented method is able to map urban land cover dynamics accurately. The performance of the presented method is further analyzed in Table 4, where detailed accuracy indicators from the confusion matrices are displayed.

Table 4. Detailed accuracy indicators of the related methods.

	OA (%)	Kappa Coeff.	Producer's Accuracy (%)					User's Accuracy (%)				
			Built-Up	Forest	Water	Bare Land	Crop Land	Built-Up	Forest	Water	Bare Land	Crop Land
SY	94.26	0.9215	91.98	98.61	98.11	92.00	87.88	98.41	100	88.14	93.88	86.57
MCY	84.15	0.8084	81.08	96.59	97.18	86.49	52.05	89.55	92.39	98.57	47.76	80.85
MI	87.76	0.8573	89.50	94.17	98.66	75.25	84.50	78.17	91.08	96.93	100	80.48
OBST	91.94	0.8879	86.15	95.83	96.04	93.39	83.19	97.22	95.74	89.82	96.47	87.85

For the MI classification, the producer's accuracies of bare land and cropland and the user's accuracy of built-up and cropland, are much lower than those in the SY, suggesting that the related indices are not able to distinguish the above types clearly enough. The image index could be considered as a dimension reduction method for distinguishing certain land cover types by transforming the principle information into one dimension. However, this transformation is often very difficult, due to the high complexity, similarity and mixture of spectral response patterns between pixels. Furthermore, indices are sensitive to dynamics of ground surface and atmospheric situation (i.e., cloud or haze). What is worse, the process of extracting a type from an index image is usually not independent of the other types. For instance, bare land, forest and cropland are extracted from the NBLI image, so that errors occurring in one step also affect the following steps.

The table suggests that the performance of OBST method is very close to the performance of SY and much better than MI. It is suggested that the land cover dynamics cannot be completely recorded and modeled in image, due to the high complicated surrounding impact factors. In Table 4, both the producer's and user's accuracies of cropland are much lower than other classes. Considering that cropland is actually a mixture of various herbaceous vegetation types, its spectral patterns are very complex. On the one hand, the spectral characteristics of some pixels in one class may be similar to other classes. Specifically, wet cropland is similar to water bodies, dry and fallow cropland is similar to bare land, dense cropland is similar to forest and so on. On the other hand, the differences among pixels within the type may be very large, for example, the difference between fallow cropland and dense cropland. Consequently, it is difficult to classify cropland accurately. Generally speaking, forest, water and bare land have relatively homogeneous physical characteristics and spectral patterns and the differences between them are relatively clear. Therefore, their accuracies are higher than cropland. Although some built-up pixels may be a mixture of impervious surface, grasses, trees, ponds and so forth, most of them have similar or homogeneous spectral patterns, guaranteeing higher classification accuracy. To improve the accuracy of sample transfer based classification, mixed pixel analysis should be considered in future studies.

4.3. Land Cover Dynamics of the Study Site

The times series land cover maps of the city derived from the Landsat images are shown in Figure 5. Based on visual inspection, the classification results well capture the spatial patterns of land covers in each year. Forests were clustered in the eastern mountainous areas and water areas were relatively unchanged during these years, benefiting from the environmental protection policies in China. At the same time, urbanization in Guangzhou is evident, as the built-up area is largely expanded to the north, east and south of the urban core. The built-up area in Guangzhou almost continuously increased from year to year and the derived areas of built-up area for the downtown of Guangzhou city in 2016 were nearly two times of that in 2001.

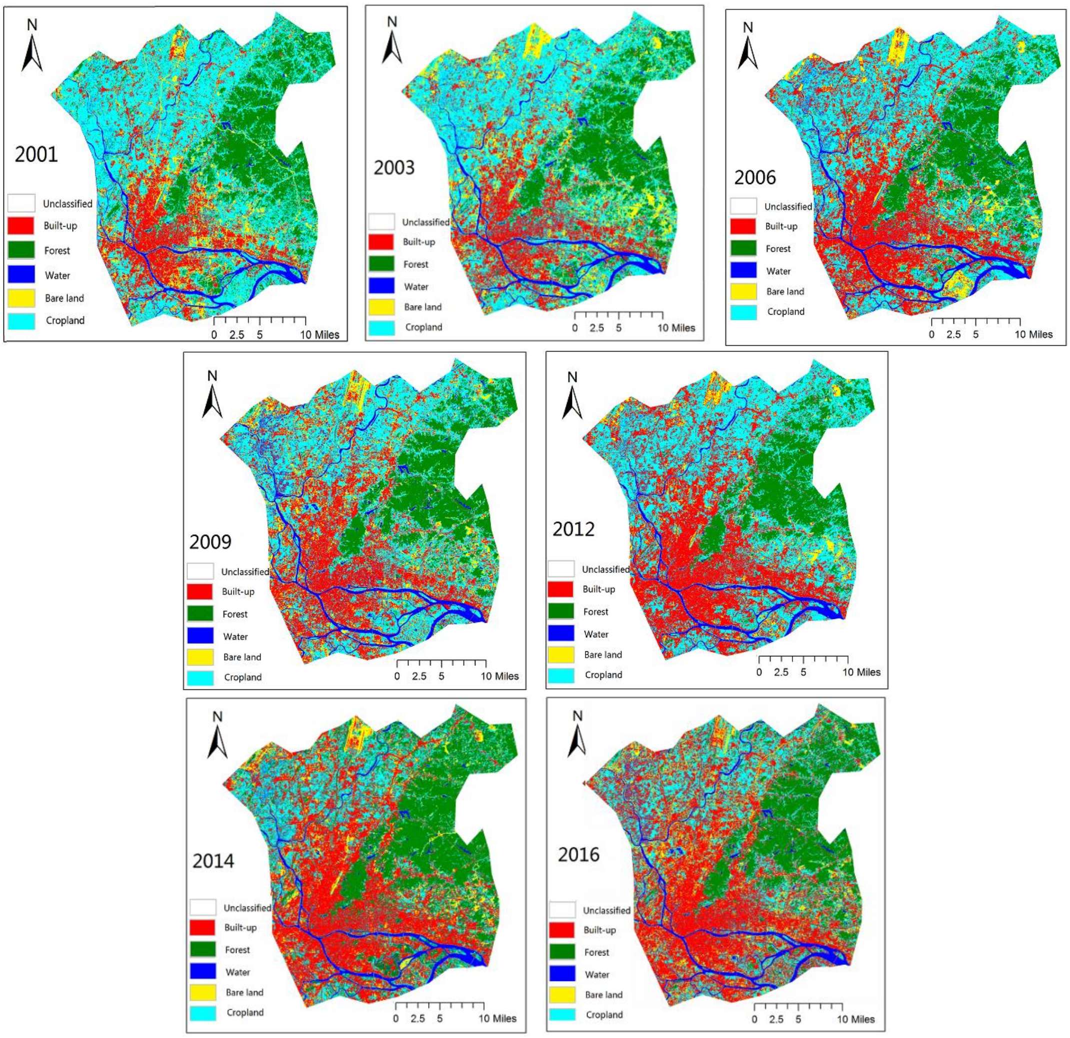

Figure 5. Land cover dynamics of the city from 2001 to 2016.

According to Figure 6, built-up areas in Guangzhou have increased rapidly since 2001. The derived built-up areas were approximately 260 km^2 in 2001 and reached to above 560 km^2 in 2016. When fitting with a simple linear trend, the annual growth rate of the built-up areas derived from Landsat images was approximately 20 km^2 per year from 2001 to 2016. Although the built-up areas appeared to increase continuously during the past 15 years in Guangzhou, the increasing rates could vary in specific periods. For example, there were slight slow-growing periods in 2001–2006 and fast-growing periods in 2006–2016. The uneven growing rates of built-up areas in the study period were likely related to the immigration of rural population into Guangzhou in previous studies [41]. At the same time, croplands have experienced dramatic decrease since 2001. The derived cropland areas were approximately 670 km^2 in 2001 but reduced to about 420 km^2 in 2016. The annual decline rate of the cropland areas derived from Landsat images was approximately 16.7 km^2 per year in these years. The dynamics of other types, that is forest, water and bare land, were not so clear and remarkable.

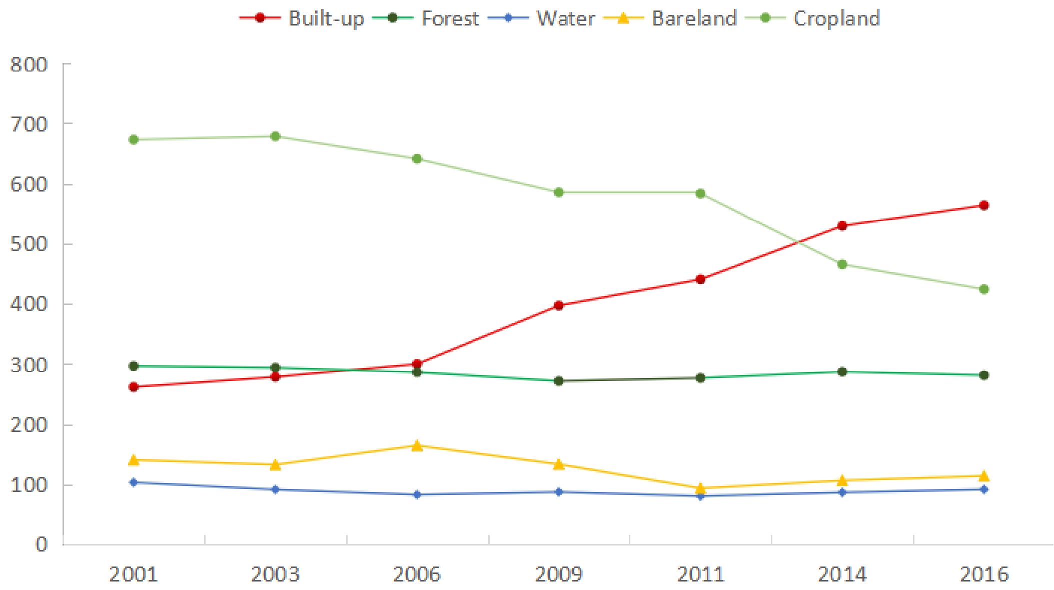

Figure 6. The variation of the land cover areas as derived from the Landsat images.

The study reveals that Guangzhou has undergone rapid urban expansion and the majority of new built-up areas are previously croplands. This suggests that the pressure on natural resources has increased in the city to meet the growing demand for built-up area. As urbanization requires more and more built-up areas for housing, business and transport infrastructure, it is generally being met through the development of natural lands (e.g., agriculture lands, forests, water bodies and so on), which ultimately results in a considerable reduction in the open and green areas of that region. How urban expansion interacts with social economy and exerts impacts on environmental sustainability is beyond the scope of the current study but is of interest to investigate with synthesized modelling in the future research.

5. Discussion

5.1. Characteristics of the Proposed Method

Due to the rapid development of Earth observation techniques, it becomes convenient to obtain a large number of remotely sensed imagery over a certain area at different times, from hundreds of Earth observation platforms However, this brings challenges that how to timely process the big remote sensing data, in terms of rapidly transferring the data into information and then knowledge. In last decades, supervised classification methods are mainly adopted for mapping land cover change However, algorithms and parameters specified for classifications at certain time are probably not suitable for those at other time or other sites, no matter how well the classifier is developed. Collecting reference data and training sample sets are always necessary for each single mapping, which often costs considerable time and budget. Thus, it becomes very difficult to monitor land cover dynamics in multi years, as a large number of times series images have to be processed.

This study aims to test if it is possible to eliminate the need to collect reference data repeatedly from year to year by finding out the transfer strategies of samples between years. According to the knowledge transfer, the knowledge discovered from historic data (source domain) could be used to map land cover from new images (target domain). Namely, although samples in one year may be not reusable in another year, affected by atmosphere, sensor calibration, solar elevation, solar azimuth, phenology and so on, some prior experience and knowledge may be helpful for new classification with data mining method. In order to seek and distribute knowledge from prior samples and ensure its availability for future users, the number and pattern of samples' change should be analyzed and found out.

This study assumed that the change of randomly selected samples must following the dynamics of land cover, when images are carefully selected with special considering for image quality, weather conditions and cloud covers. Through carefully test and analysis, general rules about land cover dynamics in developing and developed cities are concluded that: (1) most built-up, water, forest, cropland maintain unchanged and bare land are rare in a developed city; (2) in a developing a city, most built-up, water, forest and cropland keep unchanged, bare land mainly change into built-up, while most changed crop land becomes bare land. This implies the tendency of samples' change is very clear. Then accident or human errors could be easily removed with object-based sampling algorithms, through a simple filter step (i.e., he threshold 80%). Similarly, accident errors could be reduced when using OBST method. Experiments indicates the accuracy of mapping land cover without current samples has been improved with the proposed method, which is very close to SY accuracy. This prove the OBST method could be great helpful to reduce accident and human errors in the process of sample selection and transfer.

Related to the method, only source knowledge and target image are necessary, other steps (i.e., sample selection, sample transfer and mapping) could automatic realized by extracting and fusing previous information. Especially, samples for new mapping could be automatic generated without iteratively collecting and training samples by human, which lift the level of automation and applicability. This is a novel attempt towards total automatic mapping with knowledge discover theory and remote sensing technology. Experiments illustrate this solution could be applied for automatic mapping in some cases, although the performance of proposed method are still a little lower than SY. That's because the dynamics of some pixels or objects may be different from the main pattern of their type, as they are seriously affected by complicated surrounding impact factors. Then, errors will likely occur in the process of transferring samples. In the future research, novel machine learning algorithms should be imported to discover and simulate sample transfer patterns accurately.

In order to introduce the proposed method efficiently, simple algorithms and thresholds are employed in this experiment. In practical, some more specific and effective could be used. For instance, multi-instance learning based decision tree could be used for classification and multiple analysis detection for samples change detection and so on. Then, the mapping accuracy with this transfer learning strategy could be further improved. Besides, the criterions for selecting object sample and detecting changed samples could be further developed and optimized, to improve the reliability of transferred sample. Further research will focus on improving change detection accuracy and samples' quality, and on exploiting unlabeled samples or unreliable samples. Recent years, semi-supervised learning based algorithms have been presented to deal with those samples, which should be employed in future research.

5.2. Issues of Guangzhou Urbanization

With time series images, land cover variations of Guangzhou have been mapped (as shown in Figures 5 and 6). Related results reveal that the city has undergone rapid economic, industrial and urban development in recent years, similar to other cities in China, India, Vietnam and Bangladesh [1–5]. Note that in the rapid urban expansion in Guangzhou, the majority of additional built-up and bare land are acquired by converting areas that were previously cropland. As Guangzhou is located on one of the most productive agricultural lands in China-the Pearl River Delta, this conversion from natural or agricultural land into impervious surfaces consumes not only ecosystem goods and services but also considerable food production. However, in developing countries, such as China, India, Bangladesh and Vietnam, state-led industrialization and urban growth policies have often compelled farmers to sell high-yield cropland to developers [4–9]. According to the Ministry of Land and Resources of China, the total cultivated land in Mainland China continually decreased by approximately 5.6 million hectares during last two decades [11]. Fortunately, more and stricter policies to protect cropland from urban development have been presented in recent years.

This study also reveals that the increasing level of urbanization is leading to a considerable reduction in the open and green areas, as expanding built-up areas for housing, business and transport networks, mainly come from development of natural lands (e.g., grass lands, forests, water bodies and so on). This may bring potential vulnerability to natural hazards, such as channel-bank and road-surface erosion, habitat destruction, landscape degradation and fragmentation, climate change, species extinction as well as the reduction of net primary productivity [45], which has occurred in Ho Chi Minh [4], Dhaka [2,5,7]. Besides, note numerous bare land areas emerges along with urbanization processes, which could cast irreversible impacts on the urban environment, such as air pollution and soil loss [66]. In Figure 5, it is also found that the rapid human activity results in serious landscape fragmentation, namely numerous unconnected small patches of vegetation and cultivated land, greater isolation as well as higher percentage of edge areas in patches emerges in the city [66,67], Similar to Dhaka, Bangladesh [5]. As built-up and bare land types consistently exhibited the highest mean Land Surface Temperature (LST) [66], increase in unmanaged urbanization in the city and its immediate surroundings probably led to a continuous increase in LST as vegetation and floodplains are converted into either bare land or built-up surfaces [6].

A related study [32] reveals that land cover variation changes and urban expansion of the city are governed by a combination of geographical, environmental and socio-economic factors. Rapidly growing economy provides sufficient opportunities for built-up expansion and massive migration from western China to this developing city [32]. Census data indicated that the GDP of Guangzhou was only 45.2 billion dollars in 2001, which increased to 312 billion dollars in 2016 [43], with an annual growth rate of 39.4%. In 2016, the urban population grows to 14.04 million (about half of the population of Texas), with an annual growth rate of 6.6%. Among them, about 40% of the urban population was from western or central China, like other Chinese mega-cities, Beijing [8], Shanghai and Shenzhen. The additional demand for employing and accommodating the increased immigrants becomes another driver of urban expansion [2,4,7].

Rapid urbanization, along with manufacturing industries and large number of vehicles has resulted in some environmental problems, called "urban diseases." In the plum rain season, flash flooding hazards have become a serious issue and have caused human death and damages to urban infrastructure in the city [45], similar to that in Dhaka [3]. According to the 2016 annual report from the local government [68], the annual average concentration of PM2.5 was 36 $\mu g/m^3$, 4 times higher than that of Florida and 310 days had good air quality, accounting for 84.7% of the whole year. Investigation on water quality disclosed that 70% of national monitoring streams was good, while 88.7% of 53 polluted streams could not meet the lowest water quality criterion (the Chinese V type) yet [68]. Besides, the average noise on road at night in downtown was 55.3 decibels, which is officially labeled as slightly polluted [68]. More effective economic, social and environmental policies should be developed based on in-depth monitoring and analyzing the patterns, drivers and impacts of urban expansion, in order to mitigate expansion's adverse impacts.

6. Conclusions

In this study, in order to reduce the mapping cost and improve the timeliness of the LULC dynamics of Guangzhou city, an object-based sample learning method was presented. The objected-based analysis (OBA) with strict constrains in area, shape and index value is expected to reduce sample selection bias (i.e., accident errors and human errors) in selecting and transferring samples and then improve the stability of transfer learning based mapping. For the study years of 2001–2016, when the training set was collected in the same mapping year, SY yielded accuracies higher than 93%. However, when the classifier trained in one year was applied to other years, the mean CY accuracy was about 83%. The MI accuracies were generally around 88%, higher than the MCY accuracy and close to the SY accuracy. Both the overall accuracies and detailed accuracy indicators of the presented methods were higher than MCY and MI and were very close to the SY accuracy. It is therefore suggested that the presented methods are able to map urban LULC automatically, obtaining a satisfactory performance.

With the presented methods, the times series Land cover maps of Guangzhou have been derived and analyzed. Results indicate the derived built-up areas were approximately 260 km^2 in 2001, then grew to above 560 km^2 in 2016, with a growth rate of approximately 20 km^2 per year; the derived crop land areas were approximately 670 km^2 in 2001, then reduce to about 420 km^2 in 2016, with a decline rate of 16.7 km^2 per year; the variations of other types, that is, forest, water and bare land, are not so clearly and dramatic. The study reveals that Guangzhou has underwent rapid urban expansion and the majority of new built-up areas were previously crop lands. This suggests that the pressure on natural resources and environment has increased in the city to meet the growing demand for built-up area. More effective economic, social and environmental policies should be developed to mitigate urban expansion's adverse impacts, based on in-depth monitoring and analyzing the patterns, drivers and impacts of urban expansion.

The most promising application of the proposed strategy would be analyzing times-series satellite images. Mapping spatial-temporal variations of urban land cover automatically could save considerable cost and time for processing large data sets. This provides great potential for future applications as more and more satellite observations have become available all over the globe.

Author Contributions: H.L. and Y.H. conceived and designed the experiments; W.C. performed the experiments; and C.Z. wrote the paper; C.W. provided suggestions and edited the English.

Funding: This research was funded by the CRSRI Open Research Program [CKWV2018485/KY], the Key Laboratory of space Ocean Remote Sensing and Application, SOA [201701002], and the Natural Science Foundation of China [41772352].

Acknowledgments: We'd like to appreciate the anonymous reviewers, whose comments are all valuable and very helpful for revising and improving our manuscript.

Conflicts of Interest: The authors declare no conflict of interest.

References

1. Su, S.; Xiao, R.; Jiang, Z.; Zhang, Y. Characterizing landscape pattern and ecosystem service value changes for urbanization impacts at an eco-regional scale. *Appl. Geogr.* **2012**, *34*, 295–305. [CrossRef]
2. Dewan, A.M.; Yamaguchi, Y. Land use and land cover change in Greater Dhaka, Bangladesh: Using remote sensing to promote sustainable urbanization. *Appl. Geogr.* **2009**, *29*, 390–401. [CrossRef]
3. Guan, D.; Li, H.; Inohae, T.; Su, W.; Nagaie, T.; Hokao, K. Modeling urban land use change by the integration of cellular automaton and Markov model. *Ecol. Model.* **2011**, *222*, 3761–3772. [CrossRef]
4. Kontgis, C.; Schneider, A.; Fox, J.; Saksena, S.; Spencer, H.J.; Castrence, M. Monitoring peri-urbanization in the greater Ho Chi Minh City metropolitan area. *Appl. Geogr.* **2014**, *53*, 377–388. [CrossRef]
5. Dewan, A.M.; Yamaguchi, Y.; Rahman, M. Dynamics of land use/cover changes and the analysis of landscape fragmentation in Dhaka Metropolitan Bangladesh. *GeoJournal* **2012**, *77*, 315–330. [CrossRef]

6. Moghadam, H.S.; Helbich, M. Spatiotemporal urbanization processes in the megacity of Mumbai, India: A Markov chains-cellular automata urban growth model. *Appl. Geogr.* **2013**, *40*, 140–149. [CrossRef]
7. Dewan, A.M.; Kabir, M.H.; Nahar, K.; Rahman, M.Z. Urbanisation and environmental degradation in Dhaka Metropolitan Area of Bangladesh. *Int. J. Environ. Sustain. Dev.* **2012**, *11*, 118–147. [CrossRef]
8. Li, X.; Zhou, W.; Ouyang, Z. Forty years of urban expansion in Beijing: What is the relative importance of physical, socioeconomic and neighborhood factors? *Appl. Geogr.* **2013**, *38*, 1–10. [CrossRef]
9. Byomkesh, T.; Nakagoshi, N.; Dewan, A.M. Urbanization and green space dynamics in Greater Dhaka Bangladesh. *Landsc. Ecol. Eng.* **2012**, *8*, 45–58. [CrossRef]
10. Trotter, L.; Dewan, A.; Robinson, T. Effects of rapid urbanisation on the urban thermal environment between 1990 and 2011 in Dhaka Megacity, Bangladesh. *AIMS Environ. Sci.* **2017**, *4*, 145–167. [CrossRef]
11. Xiao, L.; Yang, X.; Cai, H.; Zhang, D. Cultivated Land Changes and Agricultural Potential Productivity in Mainland China. *Sustainability* **2015**, *7*, 11893–11908. [CrossRef]
12. Ma, Y.; Wu, H.P.; Wang, L.Z.; Huang, B.M.; Ranjan, R.; Zomaya, A.; Jie, W. Remote sensing big data computing: Challenges and opportunities. *Future Gener. Comput. Syst.* **2015**, *51*, 47–60. [CrossRef]
13. Adjorlolo, C.; Mutanga, O.; Cho, M.A.; Ismail, R. Challenges and opportunities in the use of remote sensing for C3 and C4 grass species discrimination and mapping. *Afr. J. Range For. Sci.* **2012**, *5490*, 563–573.
14. Aghakouchak, A.; Farahmand, A.; Melton, F.S.; Teixeira, J.; Anderson, M.C.; Wardlow, B.D.; Hain, C.R. Remote sensing of drought: Progress, challenges and opportunities. *Rev. Geophys.* **2015**, *53*, 452–480. [CrossRef]
15. Carreiras, J.M.B.; Jones, J.; Lucas, R.M.; Gabrie, C. Land Use and Land Cover Change dynamics across the Brazilian Amazon: Insights from Extensive Time-Series Analysis of Remote Sensing Data. *PLoS ONE* **2014**, *9*, e104144. [CrossRef] [PubMed]
16. Bey, A.; Díaz, A.S.; Maniatis, D.; Marchi, G.; Mollicone, D.; Ricci, S.; Bastin, J.; Moore, R.; Federici, S.; Rezende, M.; et al. Collect Earth: Land Use and Land Cover Assessment through Augmented Visual Interpretation. *Remote Sens.* **2016**, *8*, 807. [CrossRef]
17. Hai, M.P.; Yamaguchi, Y. Urban growth and change analysis using remote sensing and spatial metrics from 1975 to 2003 for Hanoi, Vietnam. *Int. J. Remote Sens.* **2011**, *32*, 1901–1915.
18. Rodriguez-Galiano, V.F.; Chica-Olmo, M.; Abarca-Hernandez, F.; Atkinson, P.M.; Jeganathan, C. Random Forest classification of Mediterranean land cover using multi-seasonal imagery and multi-seasonal texture. *Remote Sens. Environ.* **2012**, *121*, 93–107. [CrossRef]
19. Botkin, D.B.; Estes, J.E.; Macdonald, R.B.; Wilson, M.V. Studying the earth's vegetation from space. *Bioscience* **1984**, *34*, 508–514. [CrossRef]
20. Thenkabail, P.S.; Biradar, C.M.; Noojipady, P.; Dheeravath, V.; Li, Y.; Velpuri, M.; Gumma, M.; Gangalakunta, O.R.P.; Turral, H.; Cai, X.; et al. Global irrigated area map (GIAM), derived from remote sensing, for the end of the last millennium. *Int. J. Remote Sens.* **2009**, *30*, 3679–3733. [CrossRef]
21. Zhong, L.; Hawkins, T.; Biging, G.; Gong, P. A phenology-based approach to map crop types in the San Joaquin Valley, California. *Int. J. Remote Sens.* **2011**, *32*, 7777–7804. [CrossRef]
22. Zhong, L.; Gong, P.; Biging, G.S. Efficient corn and soybean mapping with temporal extendability: A multi-year experiment using Landsat imagery. *Remote Sens. Environ.* **2014**, *140*, 1–13. [CrossRef]
23. Baraldi, A. Satellite Image Automatic Mapper™ (SIAM™)—A Turnkey software executable for automatic near real-time multi-sensor multi-resolution spectral rule-based preliminary classification of spaceborne multi-spectral images. *Recent Pat. Space Technol.* **2011**, *1*, 81–106. [CrossRef]
24. Hestir, E.L.; Greenberg, J.A.; Ustin, S.L. Classification trees for aquatic vegetation community prediction from imaging spectroscopy. *IEEE J. Sel. Top. Appl. Earth Obs. Remote Sens.* **2012**, *5*, 1572–1584. [CrossRef]
25. Zhong, L.; Gong, P.; Biging, G.S. Phenology-based crop classification algorithm and its implications on agricultural water use assessments in California's Central Valley. *Photogramm. Eng. Remote Sens.* **2012**, *78*, 799–813. [CrossRef]
26. Xu, H.Q. Modification of Normalized Difference Water Index (NDWI) to Enhance Open Water Features in Remotely Sensed Imagery. *Int. J. Remote Sens.* **2006**, *27*, 3025–3033. [CrossRef]
27. Xu, H.Q. Analysis of impervious surface and its impact on urban heat environment using the Normalized Difference Impervious Surface Index (NDISI). *Photogramm. Eng. Remote Sens.* **2010**, *76*, 557–565. [CrossRef]
28. Zha, Y.; Gao, J.; Ni, S. Use of normalized difference built-up index in automatically mapping urban areas from TM imagery. *Int. J. Remote Sens.* **2003**, *24*, 583–594. [CrossRef]

29. Li, H.; Wang, C.Z.; Zhong, C.; Su, A.J.; Xiong, C.R.; Wang, J.E.; Liu, J.Q. Mapping Urban Bare Land Automatically from Landsat Imagery with a Simple Index. *Remote Sens.* **2017**, *9*, 249. [CrossRef]
30. Li, H.; Wang, C.Z.; Zhong, C.; Zhang, Z.; Liu, Q.B. Mapping Typical Urban land cover from Landsat Imagery without Training Samples or Self-Defined Parameters. *Remote Sens.* **2017**, *9*, 700. [CrossRef]
31. Kawamura, M.; Jayamana, S.; Tsujiko, Y. Relation between social and environmental conditions in Colombo Sri Lanka and the urban index estimated by satellite remote sensing data. *Int. Arch. Photogram. Remote Sens.* **1996**, *31*, 321–326.
32. Sun, Y.; Zhang, X.; Zhao, Y.; Xin, Q. Monitoring annual urbanization activities in Guangzhou using Landsat images (1987–2015). *Int. J. Remote Sens.* **2017**, *38*, 1258–1276. [CrossRef]
33. Rouse, J.; Haas, R.; Schell, J.; Deering, D. Monitoring Vegetation Systems in the Great Plains with ERTS. In Proceedings of the 3rd Earth Resources Technology Satellite Symposium, Washington, DC, USA, 10–14 December 1973; Volume 1, pp. 309–317.
34. Deng, C.; Wu, C. A spatially Adaptive Spectral Mixture Analysis for Mapping Subpixel Urban Impervious Surface Distribution. *Remote Sens. Environ.* **2013**, *133*, 62–70. [CrossRef]
35. Huang, D.; Wang, C. Optimal Multi-Level Thresholding Using a Two-Stage Otsu Optimization Approach. *Pattern Recognit. Lett.* **2009**, *30*, 275–284. [CrossRef]
36. Matasci, G.; Longbotham, N.; Pacifici, F.; Kanevski, M.; Tuia, D. Understanding angular effects in VHR imagery and their significance for urban land-cover model portability: A study of two multi-angle in-track image sequences. *ISPRS J. Int. Soc. Photogram. Remote Sens.* **2015**, *107*, 99–111. [CrossRef]
37. Tuia, D.; Persello, C.; Bruzzone, L. Domain Adaptation for the Classification of Remote Sensing Data: An Overview of Recent Advances. *IEEE Geosci. Remote Sens. Mag.* **2016**, *4*, 41–57. [CrossRef]
38. Persello, C.; Bruzzone, L. Active learning for domain adaptation in the supervised classification of remote sensing images. *IEEE Trans. Geosci. Remote Sens.* **2012**, *50*, 4468–4483. [CrossRef]
39. Persello, C. Interactive domain adaptation for the classification of remote sensing images using active learning. *IEEE Geosci. Remote Sens. Lett.* **2013**, *10*, 736–740. [CrossRef]
40. Statistic Report of Economy and Social Development of Guangzhou in 2016. Available online: http://www.gzstats.gov.cn/tjgb/qstjgb/201703/P020170331374787225515 (accessed on 11 November 2017). (In Chinese)
41. Fan, F.; Weng, Q.; Wang, Y. Land Use and Land Cover Change in Guangzhou, China, from 1998 to 2003, Based on Landsat TM /ETM+ Imagery. *Sensors* **2007**, *7*, 1323–1342. [CrossRef]
42. Fan, F.; Deng, Y.; Hu, X.; Weng, Q. Estimating Composite Curve Number Using an Improved SCS-CN Method with Remotely Sensed Variables in Guangzhou, China. *Remote Sens.* **2013**, *5*, 1425–1438. [CrossRef]
43. Zeng, C.; Shen, H.; Zhang, L. Recovering missing pixels for Landsat ETM+ SLC-off imagery using multi-temporal regression analysis and a regularization method. *Remote Sens. Environ.* **2013**, *131*, 182–194. [CrossRef]
44. Duro, D.C.; Franklin, S.E.; Dube, M.G. Multi-scale object-based image analysis and feature selection of multi-sensor earth observation imagery using random forests. *Int. J. Remote Sens.* **2012**, *33*, 4502–4526. [CrossRef]
45. Van den Eeckhaut, M.; Kerle, N.; Poesen, J.; Hervas, J. Object-oriented identification of forested landslides with derivatives of single pulse LiDar data. *Geomorphology* **2012**, *173*, 30–42. [CrossRef]
46. Dragut, L.; Csillik, O.; Eisank, C.; Tiede, D. Automated parameterisation for multi-scale image segmentation on multiple layers. *ISPRS J. Photogramm. Remote Sens.* **2014**, *88*, 119–127. [CrossRef] [PubMed]
47. Benz, U.C.; Hofmann, P.; Willhauck, G.; Lingenfelder, I.; Heynen, M. Multi-resolution, object-oriented fuzzy analysis of remote sensing data for GIS-ready information. *ISPRS J. Photogramm. Remote Sens.* **2004**, *58*, 239–258. [CrossRef]
48. eCognition. Ecognition Developer 8.0.1 User Guide. Available online: http://www.ecognition.com/free-trial (accessed on 20 October 2017).
49. Laliberte, A.S.; Herrick, J.E.; Rango, A.; Winters, C. Acquisition, Orthorectification, and Object-based Classification of Unmanned Aerial Vehicle (UAV) Imagery for Rangeland Monitoring. *Photogramm. Eng. Remote Sens.* **2010**, *76*, 661–672. [CrossRef]
50. Myint, S.W.; Gober, P.; Brazel, A.; Grossman-Clarke, S.; Weng, Q. Per-pixel vs. object-based classification of urban land cover extraction using high spatial resolution imagery. *Remote Sens. Environ.* **2011**, *115*, 1145–1161. [CrossRef]

51. Gao, Y.; Francois Mas, J.; Kerle, N.; Navarrete Pacheco, J.A. Optimal region growing segmentation and its effect on classification accuracy. *Int. J. Remote Sens.* **2011**, *32*, 3747–3763. [CrossRef]
52. Dragut, L.; Eisank, C. Automated object-based classification of topography from SRTM data. *Geomorpholgy* **2012**, *141*, 21–33. [CrossRef] [PubMed]
53. Johnson, B.; Xie, Z. Unsupervised image segmentation evaluation and refinement using a multi-scale approach. *ISPRS J. Photogramm. Remote Sens.* **2011**, *66*, 473–483. [CrossRef]
54. Di, K.; Yue, Z.; Liu, Z.; Wang, S. Automated rock detection and shape analysis from Mars rover imagery and 3D point cloud data. *J. Earth Sci.* **2013**, *24*, 125–135. [CrossRef]
55. Kitada, K.; Fukuyama, K. Land-use and land-cover mapping using a gradable classification method. *Remote Sens.* **2012**, *4*, 1544–1558. [CrossRef]
56. Racoviteanu, A.; Williams, M.W. Decision tree and texture analysis for mapping debris-covered glaciers in the Kangchenjunga area, Eastern Himalaya. *Remote Sens.* **2012**, *4*, 3078–3109. [CrossRef]
57. Haralick, R.M.; Shanmugam, K.; Dinstein, I. Textural Features for Image Classification. *IEEE Trans. Syst. Man Cybern.* **1973**, *SCM-3*, 610–621. [CrossRef]
58. Davis, L.S. A survey of edge detection techniques. *Comput. Graph. Image Process.* **1975**, *4*, 248–270. [CrossRef]
59. Huang, D.S.; Wunsch, D.C.; Levine, D.S.; Jo, K.H. Advanced Intelligent Computing Theories and Applications. With Aspects of Theoretical and Methodological Issues (ICIC). In Proceedings of the Fourth International Conference on Intelligent Computing, Shanghai, China, 15–18 September 2008.
60. Diaz-Uriarte, R.; de Andres, S.A. Gene selection and classification of microarray data using random forest. *BMC Bioinform.* **2006**, *7*. [CrossRef] [PubMed]
61. Martha, T.R.; Kerle, N.; Jetten, V.; van Westen, C.J.; Kumar, K.V. Characterising spectral, spatial and morphometric properties of landslides for semi-automatic detection using object-oriented methods. *Geomorpholgy* **2010**, *116*, 24–36. [CrossRef]
62. Bazi, Y.; Melgani, F.; Al-Sharari, H.D. Unsupervised change detection in multispectral remotely sensed imagery with level set methods. *IEEE Trans. Geosci. Remote Sens.* **2010**, *48*, 3178–3187. [CrossRef]
63. Xian, G.; Homer, C. Updating the 2001 national land cover database impervious surface products to 2006 using Landsat imagery change detection methods. *Remote Sens. Environ.* **2010**, *114*, 1676–1686. [CrossRef]
64. Gislason, P.O.; Benediktsson, J.A.; Sveinsson, J.R. Random forests for land cover classification. *Pattern Recognit. Lett.* **2006**, *27*, 294–300. [CrossRef]
65. Lawrence, R.L.; Wood, S.D.; Sheley, R.L. Mapping invasive plants using hyperspectral imagery and Breiman Cutler classifications (RandomForest). *Remote Sens. Environ.* **2006**, *100*, 356–362. [CrossRef]
66. Chen, Y.; Yu, S. Impacts of urban landscape patterns on urban thermal dynamics in Guangzhou, China. *Int. J. Appl. Earth Obs. Geoinf.* **2017**, *54*, 65–71. [CrossRef]
67. Wang, B.; Li, T.; Yao, Z. Institutional uncertainty, fragmented urbanization and spatial lock-in of the pen-urban area of China: A case of industrial land redevelopment in Panyu. *Land Use Policy* **2018**, *72*, 241–249. [CrossRef]
68. 2016 Environmental Bulletin of Guangzhou. Available online: http://www.gzepb.gov.cn/zwgk/hjgb/ (accessed on 11 November 2017). (In Chinese)